Journal of Materials Chemistry A

Accepted Manuscript

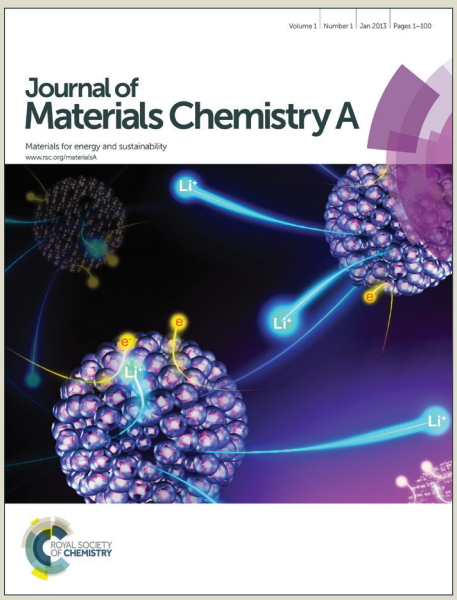

This is an *Accepted Manuscript*, which has been through the Royal Society of Chemistry peer review process and has been accepted for publication.

Accepted Manuscripts are published online shortly after acceptance, before technical editing, formatting and proof reading. Using this free service, authors can make their results available to the community, in citable form, before we publish the edited article. We will replace this *Accepted Manuscript* with the edited and formatted *Advance Article* as soon as it is available.

You can find more information about *Accepted Manuscripts* in the Information for Authors.

Please note that technical editing may introduce minor changes to the text and/or graphics, which may alter content. The journal's standard Terms & Conditions and the Ethical guidelines still apply. In no event shall the Royal Society of Chemistry be held responsible for any errors or omissions in this *Accepted Manuscript* or any consequences arising from the use of any information it contains.

ROYAL SOCIETY OF CHEMISTRY

www.rsc.org/materialsA

Journal of Materials Chemistry A RSCPublishing

ARTICLE

PAM/graphene/Ag ternary hydrogel: synthesis, characterization and catalytic application

Cite this: DOI: 10.1039/x0xx00000x

Huawen Hu, John H. Xin,* Hong Hu*

Received 00th February 2014,
Accepted 00th February 2014

DOI: 10.1039/x0xx00000x

www.rsc.org/

In this work, a ternary polyacrylamide-based composite hydrogel with functionalized graphene and silver nanoparticles was fabricated by a facile, fast and inexpensive water-based approach. The structures and catalytic properties of the prepared hydrogels with different compositions were investigated in depth. The silver ions were demonstrated to have a catalytic effect on the polymer gelation reaction which could thereby be dramatically accelerated. In addition, the low-temperature thermally functionalized graphene with a portion of oxygen functionalities and structural defect was found to play a key role in the formation of a high-performance composite hydrogel by its superior catalyst-carrying capacity and electron-transferring ability. The binary composite hydrogel without the functionalized graphene showed much lower catalytic activity as compared to the ternary counterparts, and the catalytic performance of the ternary composite hydrogel could be further enhanced by loading a higher amount of the functionalized graphene. A new cross-linking network was evidenced to be formed after incorporation of the functionalized graphene, which could enable the silver nanoparticles to be highly stabilized in the double cross-linking network matrix and thus led to the excellent reusability of the ternary composite hydrogel for several runs of catalytic reduction of different kinds of catalysants. The hydrogel catalyst could be handled much more conveniently for re-usage in different runs owing to its monolithic structure as compared to the conventional powdery catalysts. Moreover, the synergistic effect of the porous polymer network with adsorption capacity, functionalized graphene sheets having huge surface area for supporting a large number of silver nanoparticles and exceptional electron-transferring ability, and catalytically active silver nanoparticles were well demonstrated, along with a deep insight into the mechanism for the extraordinary catalytic performance of the ternary composite hydrogel.

Introduction

Metal nanoparticles (NPs) have been attracting much attention across multiple scientific disciplines including physics,[1] chemistry[2] and material science[3] owing to their unusual intrinsic properties and functionalities. Amongst the metal NPs, silver NPs are intensively studied and widely applied to a variety of areas such as electronics,[4] surface enhanced Raman spectroscopy,[5] sensing,[6] catalysis,[7] and antimicrobial[8] because of their extraordinary physical and chemical properties,[9] e.g., the high surface-to-volume ratio makes them ideal candidates for application as catalysts.[10] Unfortunately, the nano-sized silver particles tend to aggregate and agglomerate due to their high surface energy,[11] which results in much less negative Fermi potential and thus loss of the superior intrinsic properties of the silver NPs such as catalytic activity.[9] This can be explained by that the increase in particle size is generally accompanied by the increase in fraction of surface atoms in stable surface planes, and by the decrease in the proportion of atoms in low-coordination sites such as edges and corners.[12]

To address the aggregation of silver NPs, many chemical and biomolecular stabilizers have been investigated as the capping agents for stabilization of silver NPs.[13-15] However, the capping of the soft organic surfactant molecules on the active crystallographic planes of metal NPs can severely impair the superior intrinsic properties of the NPs,[16] even causing almost complete loss of catalytic properties.[17] In this regard, inorganic rigid material become a popular alternative because of the following aspects: (i) stabilization of the metal NPs; (ii) exposing sufficient quantities of active metal atoms on the clean NP surfaces; (iii) higher thermal and chemical stability as compared with soft organic stabilizer.[18,19] Among the inorganic stabilizers, graphene, a two-dimensional (2D) honeycomb sp^2-hybridized carbon network, has recently drawn an increasing attention in nanoelectronics and nanocomposites,[20] owing to its combination of giant surface area,[21] and ultra-high electron

Journal of Materials Chemistry A Accepted Manuscript

mobility,[22] thermal conductivity,[23] and mechanical strength,[24] among others.[25] Various kinds of graphene/metal NPs hybrids have been fabricated.[26-28] However, graphene aggregation has severely limited its production and applications.[29-31] Many approaches have thereby been developed to address the problems prior to its applications such as covalent[32] and non-covalent[33] modifications, and reduction of graphene oxide (GO) under given conditions.[34,35] As a result, various kinds of graphene dispersions have been produced successfully.[36-38] With effective graphene dispersions, combination of metal NPs turns to be easy through a simple and economical solution route. However, pure chemically converted graphene sheets with high extent of reduction can hardly anchor and disperse metal NPs effectively due to the lack of binding sites.[39-42] As also demonstrated in our previous paper,[43] the one-pot reduction of GO and cupric ions with hydrazine leads to large bulk of metallic copper with a micrometre size. These results reveal that the effective binding sites play an important role in formation of ultra-fine metal NPs deposited and stabilized on graphene surfaces.

Herein, given that a portion of oxygen functionalities and structural defect being present on its surfaces,[35] a mildly thermally reduced and functionalized graphene (or denoted as TrG) is expected to effectively chemisorb, complex and bind silver NPs.[44] Apart from this, a polymer network scaffold is further employed to integrate the TrG and silver NPs for addressing the following issues: (i) graphene-based monolithic composite catalyst is relatively unexplored despite the intense attention given to graphene-based hybrid powders;[26-28,39,40,42-44] (ii) the monolithic catalyst can be much more easily handled for recycling purpose relative to the powdery catalysts; (iii) an additional performance can be afforded to the resulting ternary composite monolith such as adsorption capacity of the porous network structure formed by the cross-linked polymer chains; (iv) in addition to binding with TrG, the silver NPs can be further stabilized by the confining effect from polymer network structure e.g., the amine groups of the polyacrylamide (PAM) can assist to stabilize the silver NPs grown on the TrG surfaces.[45] By considering that water is adopted as the solvent throughout the main preparation process, PAM network is selected in this study because it is cost-effective and can be produced easily by free-radical polymerization and cross-linking reaction in aqueous solution. This thereby indicates that the PAM-based ternary composite hydrogel can also be synthesized by a simple one-pot *in-situ* polymerization of the monomer acrylamide (AM), chemical cross-linking of polymer chains, and incorporation of water-soluble TrG and silver ions, followed by a mild reduction treatment for conversion of silver ions into the metallic silver NPs. In the final ternary composite, double cross-linking networks can exist: (1) the main chemical cross-linking network formed by the cross-linked polymer chains; (2) physical cross-linking network formed by the interactions between the oxygen functionalities on the TrG surfaces and amide groups of PAM chains. The double cross-linking networks afford a high-density network structure to the ternary composite hydrogel for further stabilization of silver NPs in the ternary composite.

Subsequently, a heterogeneous catalytic reduction of different kinds of catalysants with a reducing agent, $NaBH_4$, in the presence of the as-prepared hydrogel catalyst is used as a model reaction to examine the catalytic activity. Three representative catalysants are used in the present study, that is, methylene blue (MB), 4-nitrophenol (4-NP, an aromatic nitro compound), and Modern Orange 1 (MO, an azo dye). The results demonstrate that the ternary composite hydrogel shows highly efficient catalytic reduction of these catalysants and satisfactory recyclability for several runs of repeated usage. This can be attributed to the synergistic effect among the ternary components and highly stabilized silver NPs by the strong interactions with TrG and confinement effect from the double cross-linking networks. The development of the ternary composite hydrogel has therefore opened up a new avenue towards exploration of various kinds of highly efficient monolithic composite catalysts with synergistically interacted components. The work presented here will also pave the way for large-scale synthesis of binary or multicomponent composite scaffold structure with prospective applications in many fields such as tissue engineering, waste water treatment, anti-microbial, catalysis, etc.

Results and discussion

Scheme 1 depicts the main content of the present study. Structural models are created for different PAM-based hydrogels, i.e., pure PAM hydrogel, binary composite hydrogel with TrG, binary composite hydrogel with silver NPs, and ternary composite hydrogel with TrG and silver NPs. These PAM-based hydrogels show interconnected porous structure, which renders them adsorptive for catalysant molecules.[46] After incorporation of TrG into the polymer network matrix, the cavity density is believed to be increased due to the combination of main chemical cross-linking network and a new cross-linking network formed by strong physical interactions (such as hydrogen bonding) between the functional groups of the polymer chains and oxygen functionalities on the TrG surfaces. As for the binary composite hydrogel with silver NPs, long filament-like structure of the polymer is formed probably through the catalytic induction effect of silver ions in the process of simultaneous *in-situ* polymerization, corss-linking reaction, and complexation of silver ions which might lead to additional different polymerization kinetics. The filling of silver NPs into the polymer matrix affords certain catalytic activity to the as-formed binary hydrogel, while incorporation of both TrG and silver NPs into the polymer results in a highly efficient composite monolith in catalytic reduction of various kinds of catalysants including MB, 4-NP and MO.

The preparation and characterization of TrG were initially conducted in the present study before production and application of PAM-based composite hydrogels because the desired structure of TrG plays a pivotal role in successful synthesis of the well-constructed composite hydrogels with uniformly-dispersed TrG, as well as in effective anchoring of silver NPs on the TrG surfaces. A portion of oxygen-containing functional groups and structural defect are demonstrated to exist on the TrG surfaces by various characterization techniques, with the results shown in Fig. 1. Fig. 1a and 1b show the XPS spectra of GO and TrG, respectively. As shown in the XPS survey spectra of GO and TrG, the C 1s peak intensity relative to that of O 1s peak is greatly increased for TrG (C/O $\approx$ 2.07) as compared with that for GO (C/O $\approx$ 0.65), which clearly indicates that TrG contains fewer oxygen-rich functionalities than GO, but with a moderate quantity still remaining. In addition, high-resolution XPS C 1s core-level spectra of GO

Journal of Materials Chemistry A Accepted Manuscript

 This journal is © The Royal Society of Chemistry 2012

and TrG further unravel the details of the chemical bonding in GO and TrG. In the XPS C 1s spectrum of GO, there are four main deconvoluted peaks, which are centered at 284.9 (C=C/C-C), 286.7 (C-O), 287.7 (C=O) and 288.8 eV (O=C-OH). The intensities of the carbonyl and C-O peaks are significantly lower for TrG relative to that for GO, but a fair quantity of carboxyl (O=C-OH) and C-O groups are present on TrG planes. Owing to these oxygen functionalities preserved on TrG surfaces, TrG can be well-dispersed in water, as shown in Fig. 1c. Additionally, note that the colour of TrG dispersion turns black, different from the yellow brown colour of GO dispersion, which suggests the effective reduction of graphene oxide to functionalized graphene.[47] The XRD pattern of TrG is presented in Fig. 1d. As compared with GO showing a lower-angle diffraction peak (indexed to the (001) crystal plane of GO), the diffraction signals for TrG can hardly be observed, with only a small broad peak centered at $2\theta \approx 25.3^{o}$ even under magnification, which is an indication of the disordered stacking in this material.[43] While SEM and TEM images of GO show a relatively smooth plane structure (shown in Fig. 1e and 1g, respectively), increased wrinkles, folds and buckles can be found on the TrG surface (Fig. 1f, 1h), indicative of the structural defect formed in the thermal decomposition process, besides some functional groups preserved. AFM images along with the height profiles of graphene oxide and TrG shows the sheet thickness of approximately 1.03 and 1.11 nm, respectively, which thus indicates that the monolayer graphene sheets are obtained.[48-50]

With the functionalized graphene possessing a portion of oxygen functionalities and structural defect on its surfaces, the subsequent effective synthesis of PAM-based composite hydrogels can be easily carried out primarily through a water-based solution route. Various PAM-based composite hydrogels were synthesized, mainly including pure PAM hydrogel, binary composite hydrogel with TrG, binary composite hydrogel with silver NPs, and ternary composite hydrogel with both silver NPs and TrG. Fig. 2 systematically presents some details of the preparation procedure. The photo images together with the schematic illustrations of various starting materials, intermediate products and final products are clearly displayed. As can be seen, the vial (a) is charged with a given amount of monomer AM, crosslinker N,N'-Methylene-bis(acrylamide) (MBA), and solvent water (see experimental for details), and the mixture exhibits colourless transparent appearance because AM and MBA can be dissolved completely in water. Additional TrG with the concentrations of 0.6 and 1.7 mg/mL are dispersed in the mixture which correspond to the vials (b) and (c), respectively. It can be found that TrG shows good dispersion state in the solutions due to the oxygen functionalities preserved on TrG surfaces which help to solubilize TrG in water. Potassium persulfate (KPS) is used as the initiator for the free-radical polymerization of AM. After reaction at 60 ^{o}C for 4 h, the gelation of the pure PAM and binary composites with TrG can be achieved, as shown in the vials (a1), (b1) and (c1), and their washed counterparts are labelled as (a2), (b2) and (c2). It is worth pointing out that the salting out effect of KPS and the long gelation time cause the coagulation of TrG, and the aggregates of TrG can be clearly observed within the PAM matrix (see b1, c1, b2, and c2), as similarly reported elsewhere.[51] This salt effect also confirms the colloidal nature of the TrG dispersions. Unexpectedly, if silver ions are mixed into the above solutions before initiation with KPS, the gelation time can be extremely shortened. Only 5 min is needed for formation of hydrogels at room temperature, with the formed hydrogels shown in the vials (a3), (b3), and (c3). The washed counterparts are designated as (a4), (b4), and (c4). These results indicate that the silver ions act as gelation catalyst for dramatic acceleration of the gelation reaction. The extremely shortened gelation time is rather favourable for better dispersing of TrG within PAM matrix because the rapidly formed polymer network structure can immobilize TrG effectively before the adverse salt effect starts to induce the heavy coagulation of TrG. In comparison to the binary composite hydrogels without silver ions, the ternary composite hydrogels show much better dispersion of TrG within the polymer matrix, without any observable aggregates. Conversion of silver ions into metallic silver NPs are subsequently performed with the hydrazine vapour. The resulting composite hydrogels containing silver NPs are named as (a5), (b5) and (c5), which correspond specifically to binary composite hydrogel with silver NPs (PAM/Ag), ternary composite hydrogels with silver NPs and TrG at lower (PAM/0.6G/Ag) and higher (PAM/1.7G/Ag) loading levels.

Fig. 3 shows the FTIR spectra of various as-synthesized PAM-based hydrogel samples after oven-drying/dehydration treatment. Before polymerization, monomer AM presents plenty of intense absorption peaks, which reflects the feature of small molecule.[52] The typical adsorption peak centered at ~840 cm^{-1}, which can be assigned to the $=CH_2$ groups for AM,[53] disappears completely after polymerization reaction and formation of polymer PAM. This is an indication of the absence of AM in the final polymer matrix. PAM-based specimens show fewer peaks as compared to AM. Typically, two bands at about 1625 and 1599 cm^{-1} can be indexed to the amide-I (C=O stretching) and amide-II (NH bending) of PAM, respectively, together with the absorptions at 3335 and 3183 cm^{-1} which correspond to the asymmetrical and symmetrical NH stretching vibrations, respectively.[19,54] Besides, the scissoring and twisting vibrations of CH_2 can be found around 1452 and 1325 cm^{-1}, respectively.[55] It is recognized that no significant difference can be discerned between the FTIR spectra of the pure PAM and binary composites with TrG (including PAM/0.6G and PAM/1.7G), which indicates that there is virtually no chemical bonding between TrG and PAM.[56,57] Nevertheless, the presence of hydrogen bonding between them can cause a shifting of the typical band of NH to the lower wavenumber as reported in the Ref.[58] This shifting cannot be observed for the binary composites PAM/0.6G and PAM/1.7G, probably due to the heavy aggregation of TrG within the PAM matrix and thus significantly weakened hydrogen bonding interactions between TrG and PAM. This is in good agreement with the photo images presented in Fig. 1. By contrast, the FTIR spectra of the ternary composite with TrG and silver ions and its reduced counterpart with TrG and silver NPs, denoted as TrG/1.7G/Ag^{+} and TrG/1.7G/Ag, respectively, show the shifting towards lower wavenumbers from ~3335 cm^{-1} (for pure PAM) to ~3318 and 3332 cm^{-1}, respectively. This can be ascribed to the dissociation of the hydrogen bonds formed among the amide groups in the polymer.[59,60] On another hand, no apparent shifting of these peaks can be observed for both the binary composite with silver ions and its reduced counterpart (designated as PAM/Ag^{+} and PAM/Ag, respectively) relative to that for pure PAM. It can be concluded that there exist strong hydrogen-bonding interactions between the polymer chains and the well-dispersed TrG in the ternary composites, which can thereby heavily disturb the physical interactions among polymer chains themselves.[61] Further reduction with hydrazine vapour leads to the shifting towards higher wavenumber from ~3318 cm^{-1} for TrG/1.7G/Ag^{+} to ~3332 cm^{-1} for TrG/1.7G/Ag possibly due to the partial removal of functional groups. Moreover, two interesting peaks can be observed at ~814 and 1038 cm^{-1} which can

Journal of Materials Chemistry A Accepted Manuscript

be attributed to the Ag-O stretching mode caused by multiphonon processes.[62,63] These peaks show the most prominence for the binary composite PAM/Ag^+, as shown in the FTIR spectra with a selected range of wavenumber from ~1200 to 650 cm^{-1}. After reduction treatment for PAM/Ag^+, the peaks turn to be lowered in intensity as for the reduced counterpart PAM/Ag, which suggests the decreased number of Ag-O bonds. It is of interest to note that the peaks almost disappear even before the reduction treatment for ternary composite PAM/1.7G/Ag^+, and the peaks disappear completely as for the reduced counterpart PAM/1.7G/Ag. These results suggest that TrG can assist the reduction of silver ions, and even can directly partially reduce them since it has been reported that silver ions can be reduced directly by GO and reduced-GO substrates.[64]

Fig. 4 shows the XRD patterns of the various PAM-based hydrogels after oven-drying/dehydration treatment. Note that many sharp diffraction peaks can be observed for the monomer AM, indicating its crystalline nature. In contrast, as for pure PAM and its binary composites with TrG, only weak amorphous diffraction peaks can be found, which indicates that they are completely amorphous. This can be explained by the random crosslinking of the PAM molecules, instead of regular molecule arrangement. Concerning PAM/Ag^+, oxides of silver, including AgO and Ag_2O are demonstrated through its XRD pattern. In addition, a trace amount of the metallic silver are confirmed by the weak signal of face-centred cubic (fcc) silver (JCPDS file no. 04-0783). It is interesting to note that the incorporation of TrG can reduce the oxides of silver to a certain extent, as evidenced by the weaker intensity of the bands of the oxides and stronger intensity of the bands of the metallic silver. The increase of the TrG content leads to a higher extent of reduction. These results are in good agreement with FTIR spectra. Moreover, as for PAM/Ag being further processed by hydrazine vapour, the XRD signals of the oxides of silver almost disappear, along with a much stronger intensity of the diffraction bands associated with the metallic silver as compared to that for PAM/Ag^+. The signals from the metallic silver become even stronger for the ternary composites PAM/0.6G/Ag and PAM/1.7G/Ag as compared with that for PAM/Ag, especially for the ternary composite with the higher loading dose of TrG, which is attributed to the higher quantities of silver NPs carried by TrG and immobilized in the double cross-linking networks. These results indicate that TrG can effectively support a large number of silver NPs on its surfaces through the first adsorption of silver ions by electrostatic and complexation interactions with the portion of the functional groups and structural defect existing on the TrG surfaces,[65] and then highly efficient reduction of these ions into metallic silver contributed by reduction electron-transferring property of TrG. Moreover, TrG can even directly reduce the oxides of silver to a certain extent. The remarkable intrinsic properties of TrG are therefore well demonstrated, such as huge surface area, catalyst-carrying capacity and ultra-high electron mobility.

SEM morphology observation of the freeze-fractured sections of the lyophilized pure PAM, PAM/Ag and PAM/1.7G/Ag is presented in Fig. 5. As expected, pure PAM shows high porosity, with different cavity sizes (Fig. 5a,5b). Such porous structure is expected to afford excellent adsorption property to the PAM hydrogel.[66,67] The interconnected cavity with different sizes can perhaps make it adaptable to different-sized molecules used as the adsorbates. The corresponding structural model are also presented to unravel the structure feature of the polymer network marked in bluish violet shading. In the SEM images of ternary composite hydrogel with TrG and silver NPs (Fig. 5c,5d), a totally different section morphology can be identified from that of the pure PAM. The sheet-like structure indexed to the component TrG can be clearly observed and is highlighted in green shading. It is noted that TrG is well dispersed in the polymer network matrix. Moreover, a large number of silver NPs are evenly decorated on the graphene surfaces (highlighted by red shading), except for a piece of silver aggregate which can be seen on the fractured surface and seems to be free of bonding with TrG (highlighted by dashed red circles). The existence of this aggregate implies the strong holding powder provided by the double cross-linking networks. Otherwise, the aggregate should be removed out of the network by strong washing post-treatment. EDX spectrum of the ternary composite shown in Fig. 5e further confirms the presence of silver composition through the detected signal of silver element. To further demonstrate the composition of the sheet-like structure, EDX mapping images along with the corresponding SEM image are given in Fig. 5f-5i. The result confirms the existence of C, O, and Ag elements in the sheet-like structure examined, which corresponds well to the composition of the functionalized graphene decorated with silver NPs. In addition, it is evident that the silver NPs are homogeneously distributed over the surface of the sheet-like structure. In comparison to PAM/1.7G/Ag, the SEM images of the binary composite PAM/Ag display a completely different section morphology (Fig. 5j,5k). The sheet-like structure can no longer be observed due to the absence of TrG. Instead, numerous filament-like structures are generated and intertwined together into a new network structure, which might be attributed to that the silver ions make a new reaction path for PAM. This likely explains the substantially increased reaction rate after incorporation of silver ions. On the other hand, there are no silver particles that can be identified in the SEM images for PAM/Ag, although silver composition can be confirmed by the EDX spectrum (Fig. 5l). These results imply that TrG plays a very important role in carrying and supporting silver NPs. Only the single polymer network can hardly immobilize silver NPs, which is in line with the XRD and the following TEM results.

TEM is further provided to demonstrate the silver aggregate which is free of bonding with TrG and is imprisoned in the double cross-linking networks (highlighted by dashed red cycles in the SEM images and schematic diagram of PAM/1.7G/Ag). This aggregate can be released from the networks after opening the confining network through pulling apart the integrate hydrogel into several pieces and exposing the aggregate. Additionally, the filament-like structure of PAM/Ag (found in the SEM images) is also verified. To release the silver aggregate out of the network, the wet hydrogel PAM/1.7G/Ag was pulled apart into several pieces and dispersed into water, and the dispersion was dropped onto a carbon-coated copper grid for the TEM observation (Fig. 6a-6d). Only very limited number of free particles could be found on the copper grid, without any graphene- and polymer-like structures, indicating the overall high compatibility and combination among the components. The several NPs (with an average diameter of about 60 nm) found in Fig. 6b is believed to be generated from the silver aggregate like the one observed in the SEM cross-sectional images. The preparation process for the TEM specimen was likely to cause the big aggregate to be disaggregated into some smaller NPs as schematically shown in Fig. 6a. The HRTEM image (Fig. 6c) demonstrates the crystalline fcc silver structure for the particle through measurement of interplanar spacing from the clear lattice fringes. The calculated value is ~0.23 nm, which can be

Journal of Materials Chemistry A Accepted Manuscript

 This journal is © The Royal Society of Chemistry 2012

indexed to {111} facets of fcc silver.[68] In addition, the SAED pattern (Fig. 6d) reveals that the particle has single crystal nature with cubic phase.[69] These results further demonstrate that the double cross-linking networks give sufficiently high holding power for the free big silver aggregate, and only under a strong external destructive force, did the aggregate release out of the networks. By contrast, as for PAM/Ag, completely different results can be noted (Fig. 6e-6g). There is no free silver NPs that can be seen on the copper grid, with only long filament-like structures observable. The filament-like structures correspond well to those found in the SEM images. In addition, a few silver NPs dispersed in the filament matrix can be seen in the TEM images, even though they cannot be identified in the SEM images. Most bodies of these silver NPs are embedded in the polymer matrix, with limited "naked" surfaces exposed. These results indicate that silver NPs cannot be held only by the single polymer network without TrG. Otherwise, free silver NPs can be observed since the destruction of polymer network can release the confined silver NPs. This thereby suggests the marked importance of the double cross-linking networks for immobilization and stabilization of silver NPs. Although a few silver NPs can be found in the filament-like polymer matrix, the content is too low to impart a high catalytic activity to PAM/Ag. Even worse, most bodies of these NPs are embedded in the polymer matrix, which is an indication that the limited active "naked" surfaces of the silver NPs can be accessed, resulting in a very low catalytic activity.[16,17]

The catalytic activities of the PAM-based composite hydrogels are subsequently evaluated by a model reduction reaction using $NaBH_4$ as the reducing agent, which is widely used to examine the catalytic activities of various metal NPs-based catalysts.[10,43,70] Catalytic reduction of commonly used dye MB is first performed, with the results shown in Fig. 7a-7j. Fig. 7a gives the molecular structure of MB. As aforementioned, the high porosity can make the PAM hydrogel adsorptive, which is further verified in Fig. 7b. After 24 h of adsorption interaction, the color of the starting MB becomes much lighter, while the original colorless PAM hydrogel turns to be colored in blue owing to the adsorbed MB molecules within the porous polymer network. Fig. 7c presents the result of the catalytic reaction between the reducing agent and MB in the absence of any catalyst. The reaction proceeds very slowly, 6 h of reaction leads to the MB solution still highly colored, with slightly changed typical UV/vis absorption peak intensity (centered at approximately 662 nm). In the presence of the catalyst PAM/Ag, the reaction between MB and $NaBH_4$ can be expedited indeed, but it still takes 2.5 h to approach the end of the reaction which is reflected by the color almost entirely faded and the typical UV/vis absorptions disappeared (Fig. 7 d). As expected, in the presence of the catalyst PAM/0.6G/Ag or PAM/1.7G/Ag, the reaction rate is increased dramatically. Both of the reaction systems with the ternary composite hydrogels examined can reach the end of reaction within only 80 s, as confirmed by the completely faded colour and totally vanished typical UV/vis absorptions (Fig. 7e,7f). It is worth pointing out that the reaction can be completed basically within 40 s for the ternary composite hydrogel containing higher concentration of TrG, namely PAM/1.7G/Ag (Fig. 7f), whereas 40 s is insufficient to complete the reaction for the ternary composite hydrogel with lower content of TrG, in this case PAM/0.6G/Ag (Fig. 7e). In these catalytic reactions, owing to the fact that $NaBH_4$ was in excess as compared with MB, the reaction rate was roughly independent of the $NaBH_4$ concentration, and the kinetics can be considered pseudo-first-order with respect to MB.[71] Fig. 7g plots $ln\ (A_t/A_0)$ as a function of reaction time for the three different catalysts, where A_t and A_0 is the peak intensity at time t and 0, respectively (the right magnified Figure shows the plots for the systems with the ternary composites PAM/0.6G/Ag and PAM/1.7G/Ag to clearly present their difference). The linear relationship confirms the pseudo-first-order kinetics, and the kinetic rate constant is estimated from the slope as 0.040, 2.951, and 3.056 min^{-1} for PAM/Ag, PAM/0.6G/Ag, and PAM/1.7G/Ag, respectively. These results indicate that the ternary composite hydrogels have much higher catalytic activity than the corresponding binary composite hydrogel owning to the fact that the extraordinary properties of TrG, particular for the catalyst-carrying property, have been integrated into the ternary composites. In addition, the synergistic effect of the three components plays another significant role in the remarkably high catalytic activity of the ternary composites. Furthermore, the discoloured solutions after the catalytic reaction were investigated by shaking of the vials loaded with the faded solutions, with the results shown in Fig. 7h. It is of interest to find that blue colour reemerges as for the reaction system with PAM/Ag, while the color reemergence cannot be found for both the reaction systems with ternary composite hydrogels, namely PAM/0.6G/Ag and PAM/1.7G/Ag. This can be further evidenced by the UV/vis results that the typical absorption peak of MB reemerges for the reaction system with PAM/Ag, whereas almost no absorption changes can be found for the systems with PAM/0.6G/Ag and PAM/1.7G/Ag. This indicates that catalytic reduction reaction is concomitantly accompanied by the adsorption provided by the porous structure of the polymer network, and this adsorption plays an important role in discoloration of MB, especially for the system with PAM/Ag. Due to the lack of the sufficient silver NPs with active "naked" surfaces exposed, PAM/Ag cannot thoroughly catalytically reduce MB at a given time period. In contrast, a sufficient number of well-dispersed silver NPs carried by TrG can render the ternary composites highly active for catalytic reduction of MB, which thus results in the fully reduced MB. It is worth mentioning that the composite hydrogels can be recycled conveniently after catalytic reaction because of its monolithic structure, much superior to the graphene-based catalyst in powder form. This is also illustrated schematically in Figure 7i. Moreover, to test the recyclability of the composite hydrogels, the typical composite hydrogel, PAM/1.7G/Ag, was recycled and reused for total 5 runs. The result is depicted in Fig. 7j. Even after 5 runs of usage, the catalytic efficiency remains sufficiently high (over 90% relative to the 1st run). The good reusability can be attributed to the highly stabilized silver NPs in the double cross-linking networks of the ternary composite.

In addition to MB, another important catalysant used in this study is an organic aromatic nitro compound, in this case 4-nitrophenol (4-NP). Among various aromatic nitro compounds, 4-NP is one of the mostly produced by-products, which is contaminant to the environment.[72] Moreover, in pharmaceutical industries, 4-aminophenol (4-AP) is always produced by reduction of 4-NP. The 4-AP is well known as a very important precursor for the production of a variety of medicines such as acetanilide paracetamol, antipyretic and phenacetin drugs.[70] It is also widely developed as corrosion inhibitor, photographic developer, hair-dyeing agent, and anticorrosion-lubricant.[73] The investigation on the catalytic reduction of 4-NP therefore shows great value across different fields. The results of the catalytic reduction using the typical PAM/1.7G/Ag as the catalyst are shown in Fig. 8(a)-8(c). Fig. 8(a) presents the structural models of 4-NP and its reduced counterpart 4-AP, together with the corresponding photo images showing the aqueous solutions of 4-nitrophenolate ion (converted from 4-NP after addition of $NaBH_4$) and of 4-AP after the catalytic reduction with PAM/1.7G/Ag. The solution of 4-nitrophenolate ion displays a bright yellow color, and it turns colorless after the catalytic reduction due to the conversion of 4-NP to 4-AP. It can be found in Fig. 8(b)

Journal of Materials Chemistry A Accepted Manuscript

that it takes only 90 s to complete the catalytic reduction, as evidenced by the discolored solution, totally vanished absorption peak at about 400 nm which can be indexed to 4-NP, and concomitantly emerged absorption peak at around 300 nm which can be assigned to 4-AP.[74] The reusability test for the PAM/1.7G/Ag also shows a highly satisfactory result after 5 runs of catalytic reduction of 4-NP, as shown in Fig. 8(c).

The last catalysant employed in the present study is an azo dye, in this case MO. Azo-based dyes represent a major category of dyes and are widely applied in coloration industry. The effluents containing azo-based dyes generated from the coloration processes are considered a serious water pollutant by considering their toxicity, and that, even worse, some derivatives of azo-based dyes are carcinogenic.[75,76] The study on catalytic reduction of azo-based dye is herein highly important in material and environmental science. The results of catalytic reduction of MO using PAM/1.7G/Ag as the catalyst are presented in Fig. S1(a)-S1(g). Fig. S1(a) depicts the molecular structure of MO. In the absence of the catalyst, the color of aqueous solution of MO is changed gradually from the starting yellow to a dark red after the reaction between MO and $NaBH_4$ for 20 h (Fig. S1(b)), which can be indexed to the new UV/vis adsorption band appeared at approximately 487 nm (Fig. S1(c)). On the contrary, in the presence of the catalyst, the yellow color of MO solution is deepened initially to yellow brown, followed by stepwise fading to be colorless (Fig. S1(d)). The discoloration process can be tracked by UV/vis spectroscopy, with the result shown in Fig. S1(e). The typical absorption peak centered at about 372 nm disappears gradually with reaction time. From the plot of A/A_0 versus reaction time shown in Fig. S1(f), the reaction practically reaches the end after 6 h. In this case of the catalytic reduction of MO, a satisfactory reusability test result is also obtained (Fig. S1(g)).

Finally, the mechanism is provided to explain the highly efficient ternary composite hydrogel towards catalytic reduction of different types of catalysants. Because of its importance in the catalytic reductions as aforementioned, the adsorption capacity of the PAM-based hydrogel for all the catalysants used in this study is first demonstrated. After impregnation of the PAM hydrogel in the aqueous solution of each catalysant for 24 h, the processed hydrogel shows the highly colored body with the corresponding color of the catalysant solution where it was impregnated, as shown in Fig. S2. This result indicates that the PAM hydrogel can effectively adsorb different types of catalysants into its highly porous structure (with different cavity sizes) that has been verified by SEM. The result is also consistent with the related study involving using PAM-based hydrogel as a good adsorbent for various kinds of dyes.[77,78] The possibility for the catalysant molecules to penetrate into the inside of the interconnected PAM network structure is significant for the effective adsorption and thus gives the intense catalytic reduction reaction. The evolution of the adsorption of the catalysant molecules into the PAM network is also schematically presented in Fig. S2. Furthermore, we use another schematic structural illustration to unveil the adsorption and catalytic reduction of dyes by the ternary composite hydrogel, as shown in Scheme 2. The adsorption capacity enables the catalysant molecules to be approached around the graphene sheets and the active silver NPs more quickly. Moreover, the graphene can rapidly shuttle the reduction electron offered by the reducing agent to the silver NPs deposited on the graphene surfaces. These synergistic interactions make the catalytic reduction proceed violently. More specifically, the electrophilic catalysant molecules approached around and attached to the silver NP surfaces leads to the increase of the Fermi potential of the silver NPs and thus the decrease of the difference in the potential between the silver NPs and the catalysant. This actually does not favor the catalytic reduction since the larger the difference between the two potentials, the higher is the catalytic reaction rate.[79] However, when the reduction electrons offered by the reducing agent are rapidly transferred to silver NPs with the assistance of the graphene sheets possessing superior electron-transferring ability, the Fermi potential of the silver NPs is decreased sharply, along with the markedly increased potential difference between the silver NPs and the catalysant. As a result, the highly efficient reduction of the catalysant is achieved. Therefore, the synergistic effect of polymer network, TrG and silver NPs is well demonstrated for contribution to the highly efficient catalytic reduction reaction. The schematic explanation of the synergistic interaction mechanism is given in Scheme 3.

Experimental

Materials. Acrylamide monomer (A.R. grade), N,N'-Methylene-bis(acrylamide) (99%), and potassium persulfate (A.R. grade) were supplied by Sigma-Aldrich. Graphite fine powder (Extra pure) and silver nitrate (A.R. grade) were obtained from Tianheng Technology Co., Ltd., Hong Kong. All other chemicals were commercial products of A.R. grade and purchased from Sigma-Aldrich and Tianheng Technology Co., Ltd. All the chemicals were used as received without further purification.

Synthesis of GO. GO was synthesized by a modified Hummers method as described elsewhere.[80] Typically, graphite fine powder (2.0 g) and $NaNO_3$ (1.0 g) were charged into a 250 mL flask, followed by gradual addition of 50 mL of concentrated H_2SO_4 under magnetic stirring and cooling using an ice bath. The mixture was kept stirring at 5 ^oC for 2 h. Afterwards, 7.3 g of $KMnO_4$ was added slowly under cooling and continuously stirring to keep the temperature of the suspension lower than 20 °C. After feeding $KMnO_4$, the temperature was raised to 35 ^oC, followed by continuously stirring for 30 min. Deionized (DI) water (90 mL) was then added in small portions, and the mixture was stirred for another 15 min. An additional 55 mL of DI water was added followed by a slow addition of 7 mL of H_2O_2 (30%) in order to reduce residual permanganate to soluble manganese ions. Finally, the mixture was filtered and thoroughly washed with diluted HCl (5%, 150 mL), DI water (150 mL) and methanol (150 mL), followed by drying treatment under vacuum at 50 ^oC for 24 h.

Preparation of TrG. A given amount of the as-synthesized GO was placed in a ceramic container, followed by insertion of the container into a muffle furnace which was preheated to 400 ^oC and saturated with nitrogen atmosphere beforehand. After holding at the temperature for 30 s, the furnace was cooled down to room temperature. The ceramic container was then withdrawn, and the functionalized graphene sheets, namely TrG, were collected for the subsequent experiment.

***In-situ* synthesis of ternary composite hydrogel.** The as-prepared TrG (0.6 mg) was dispersed into 10 g of DI water by ultrasonication (150 W) for 1 h. The monomer acrylamide (AM) (1 g) was then dissolved in the TrG dispersion by mild stirring, followed by dissolving 7 mg of N,N'-Methylenebis(acrylamide) (MBA) which was used as the chemical cross linker. Before initiation of the free-radical polymerization of AM with potassium persulfate (KPS, 11 mg), 2 g of $AgNO_3$ was dissolved into the suspension. The free-radical polymerization and cross-linking gelation reactions were carried out at room temperature. The PAM-based ternary composite hydrogel with TrG and silver ions (denoted as PAM/0.6G/Ag^+) was formed within 5 min. The PAM/1.7G/Ag^+ was also prepared similarly according to the above procedure only by increasing the loading amount of TrG from 6 to 17 mg.

Journal of Materials Chemistry A Accepted Manuscript

 This journal is © The Royal Society of Chemistry 2012

Further conversion of silver ions to silver NPs was conducted by treating the slices (which were cut from the as-prepared composite hydrogels) with hydrazine vapour for 12 h. The treated PAM/0.6G/Ag^+ and PAM/1.7G/Ag^+ are termed as PAM/0.6G/Ag and PAM/1.7G/Ag, respectively. For comparison, the binary PAM composite hydrogel with Ag^+ before and after the post-treatment with hydrazine vapour were similarly prepared except that TrG was not added. The resulting binary composite hydrogels before and after processing with hydrazine vapour were named as PAM/Ag^+ and PAM/Ag, respectively. In addition, the binary PAM composite hydrogels with TrG were also similarly prepared except that silver nitrate was not loaded and the polymerization and cross-linking gelation reactions were conducted at 60 °C for 4 h. These as-prepared binary composite hydrogels with TrG are denoted as PAM/0.6G and PAM/1.7G accordingly. The pure PAM hydrogel was also prepared in the absence of TrG and silver nitrate based on the above procedure.

Catalytic activity measurement. To study the catalytic activity, a small slice of the composite hydrogel sample was used as the catalyst for the catalytic reduction of different kinds of catalysants in aqueous solution using $NaBH_4$ as reducing agent. Typically, the as-prepared composite hydrogel PAM/1.7G/Ag (0.13 g) was added to the 8 ml of MB solution (0.1 mM), followed by addition of $NaBH_4$ (10.0 mg). Digital camera and UV/vis spectrometer were employed to examine the extent of the reduction reaction. The catalytic reduction of MO was conducted with an identical procedure to the case with MB. As for the catalysant 4-NP, $NaBH_4$ was first added to the aqueous solution of 4-NP for conversion of 4-NP to nitrophenolate ion before the catalytic reduction of 4-NP started by addition of the composite hydrogel catalyst. In addition, reusability test for the typical composite hydrogel, PAM/1.7G/Ag, was performed after thorough washing of the recycled catalyst, and the total 5 runs of repeated usage was investigated.

Characterizations. Ultraviolet/visible (UV/vis) spectra were recorded on a Lambda 18 UV/VIS Spectrometer. X-ray photoelectron spectroscopy (XPS) measurement was performed using a Sengyang SKL-12 electron spectrometer equipped with a VG CLAM 4 MCD electron energy analyzer. Fourier transformed infrared (FTIR) spectra of the PAM-based hydrogel samples after dehydration treatment were collected using a FTIR spectrometer (Perkin Elmer System 2000), in the mode of attenuated total reflection (ATR). Powder X-ray diffraction (XRD) pattern was recorded on a Bruker D8 Advance X-ray diffractometer (Bruker AXS, Karlsruhe, Germany). The morphologies of the GO and TrG powders, and the fractured-sections of the lyophilized PAM-based hydrogels were observed by a field-emission scanning electron microscopy (FE-SEM, JEOL JSM-6335F). The lyophilisation process was conducted as follows: the hydrogel samples were pre-frozen at -196 °C in liquid nitrogen, and then lyophilized at 0.026 mbar and -60 °C for 48 h using a Heto FD8 freeze dryer. Energy-dispersive X-ray (EDX) spectra and mapping images were recorded on an INCA spectrometer attached to the SEM. Atomic force microscopy (AFM) was performed on a Nanoscope Multimode IIIa scanning probe microscopy system in the tapping mode. The specimens used for AFM test were prepared by dropping the water dispersions of various specimens onto silicon wafers, followed by drying treatment at room temperature. Transmission electron microscopy (TEM) images and selected area electron diffraction (SAED) patterns were obtained by a Jeol JEM-2011 TEM facility at an acceleration voltage of 100 kV.

Conclusions

A novel ternary composite hydrogel with low-temperature thermally functionalized graphene and silver nanoparticles has been fabricated and demonstrated to be highly efficient in catalytic reduction of different kinds of catalysants including methylene blue, 4-nitrophenol and an azo dye. The silver ions are confirmed to have a catalytic effect on the gelation reaction which can thereby be surprisingly accelerated for formation of the composite hydrogels. In addition, the functionalized graphene is evidenced to act as a pivotal component for generation of high-performance ternary composite hydrogels owing to its superior catalyst-carrying capacity and reduction electron-transferring ability. Moreover, in addition to the chemical cross-linking network formed by the cross-linked polymer chains, a new cross-linking network is generated through the strong hydrogen bonding interactions between the functional groups of polymer chains and oxygen functionalities on the graphene surfaces as for the ternary composite. These double cross-linking networks are probably responsible for the highly stabilized silver nanoparticles and thus the satisfactory recyclability of the ternary composite catalyst. The monolithic structure affords convenient handling property to the hydrogel catalyst for re-usage in different runs. The synergistic interactions among the ternary components play a key role in the highly efficient catalytic performance of the ternary composite, which has been well demonstrated in this study.

Acknowledgements

We acknowledge the funding from Research Grants Council (RGC) of the Hong Kong SAR Government (PolyU 5316/10E).

Notes and references

[a] Institute of Textiles and Clothing, The Hong Kong Polytechnic University, Hong Kong SAR 999077, China;
Fax: (+86) 852-2766-6474
E-mail: tcxinjh@polyu.edu.hk

Electronic Supplementary Information (ESI) available: [the results of catalytic reduction of the azo-based dye, namely MO, and digital images along with the structural models demonstrating the adsorption capacity of PAM-based hydrogel for the catalysants investigated in this study]. See DOI: 10.1039/b000000x/

1. G. Sun, J. B. Khurgin and D. P. Tsai, *Opt. Lett.*, 2012, **37**, 1583.
2. P. Barbaro, V. Dal Santo and F. Liguori, *Dalton T.*, 2010, **39**, 8391.
3. Y. Tang and M. Ouyang, *Nat. Mater.*, 2007, **6**, 754.
4. M. Rycenga, C. M. Cobley, J. Zeng, W. Li, C. H. Moran, Q. Zhang, D. Qin and Y. Xia, *Chem. Rev.*, 2011, **111**, 3669.
5. Y. C. Lai, W. X. Pan, D. J. Zhang and J. H. Zhan, *Nanoscale*, 2011, **3**, 2134.
6. V. Tharmaraj and K. Pitchumani, *Nanoscale*, 2011, **3**, 1166.
7. Y. G. Hu, T. Zhao, P. L. Zhu and R. Sun, *Colloid Polym. Sci.*, 2012, **290**, 401.
8. P. Kanmani and S. T. Lim, *Carbohyd. Polym.*, 2013, **97**, 421.
9. T. Zhang, X. Li, S.-Z. Kang, L. Qin, G.-D. Li and M. Jin, *J. Mater. Chem. A*, 2014, **2**, 2952.
10. Y. Lu, Y. Mei, M. Drechsler and M. Ballauff, *Angew. Chem. Int. Edit.*, 2006, **45**, 813.
11. L. Sun, Z. J. Zhang and H. X. Dang, *Mater. Lett.*, 2003, **57**, 3874.
12. F. Zaera, *Chemsuschem*, 2013, **6**, 1797.
13. Y. G. Sun and Y. N. Xia, *Science*, 2002, **298**, 2176.

Journal of Materials Chemistry A Accepted Manuscript

14. H. J. Hah, S. M. Koo and S. H. Lee, *J. Sol-Gel Sci. Techn.*, 2003, **26**, 467.
15. L. Kvitek, A. Panacek, J. Soukupova, M. Kolar, R. Vecerova, R. Prucek, M. Holecova and R. Zboril, *J. Phys. Chem. C*, 2008, **112**, 5825.
16. C. Xu and X. Wang, *Colloid Surf. A*, 2012, **404**, 78.
17. C. J. Huang, C. Chen, X. X. Ye, W. Q. Ye, J. L. Hu, C. Xu and X. Q. Qiu, *J. Mater. Chem. A*, 2013, **1**, 12192.
18. J. Morere, M. J. Tenorio, M. J. Torralvo, C. Pando, J. A. R. Renuncio and A. Cabanas, *J. Supercrit. Fluid*, 2011, **56**, 213.
19. H. W. Hu, J. H. Xin, H. Hu, A. Chan and L. He, *Carbohyd. Polym.*, 2013, **91**, 305.
20. S. J. He, B. Song, D. Li, C. F. Zhu, W. P. Qi, Y. Q. Wen, L. H. Wang, S. P. Song, H. P. Fang and C. H. Fan, *Adv. Funct. Mater.*, 2010, **20**, 453.
21. X. Zhang, X. Ji, R. F. Su, B. L. Weeks, Z. Zhang and S. L. Deng, *Chempluschem*, 2013, **78**, 703.
22. K. I. Bolotin, K. J. Sikes, Z. Jiang, M. Klima, G. Fudenberg, J. Hone, P. Kim and H. L. Stormer, *Solid State Commun.*, 2008, **146**, 351.
23. B. C. Lee, A. A., S. Ghosh, W. Z. Bao, I. Calizo, D. Teweldebrhan, F. Miao and C. N. Lau, *Nano Lett.*, 2008, **8**, 902.
24. C. Lee, X. D. Wei, J. W. Kysar and J. Hone, *Science*, 2008, **321**, 385.
25. Y. B. Zhang, Y. W. Tan, H. L. Stormer and P. Kim, *Nature*, 2005, **438**, 201.
26. C. Xu, X. Wang and J. W. Zhu, *J. Phys. Chem. C*, 2008, **112**, 19841.
27. J. F. Shen, M. Shi, N. Li, B. Yan, H. W. Ma, Y. Z. Hu and M. X. Ye, *Nano Res.*, 2010, **3**, 339.
28. Y. Li, X. B. Fan, J. J. Qi, J. Y. Ji, S. L. Wang, G. L. Zhang and F. B. Zhang, *Nano Res.*, 2010, **3**, 429.
29. W. F. Zhao, M. Fang, F. R. Wu, H. Wu, L. W. Wang and G. H. Chen, *J. Mater. Chem.*, 2010, **20**, 5817.
30. J. Yang, C. L. Zang, L. Sun, N. Zhao and X. N. Cheng, *Mater. Chem. Phys.*, 2011, **129**, 270
31. H. J. Song, L. Y. Hao, Y. F. Tian, X. Y. Wan, L. C. Zhang and Y. Lv, *Chempluschem*, 2012, **77**, 379.
32. C. S. Shan, H. F. Yang, D. X. Han, Q. X. Zhang, A. Ivaska and L. Niu, *Langmuir*, 2009, **25**, 12030.
33. Y. X. Xu, H. Bai, G. W. Lu, C. Li and G. Q. Shi, *J. Am. Chem. Soc.*, 2008, **130**, 5856.
34. Y. X. Xu, K. X. Sheng, C. Li and G. Q. Shi, *J. Mater. Chem.*, 2011, **21**, 7376.
35. H. Hu, C. C. Allan, J. Li, Y. Kong, X. Wang, J. H. Xin and H. Hu, *Nano Res.*, 2014, **7**, 418.
36. D. R. Dreyer, S. Park, C. W. Bielawski and R. S. Ruoff, *Chem. Soc. Rev.*, 2010, **39**, 228.
37. Y. Chen, B. Zhang, G. Liu, X. D. Zhuang and E. T. Kang, *Chem. Soc. Rev.*, 2012, **41**, 4688.
38. Z. Pan, H. L. Gu, M. T. Wu, Y. X. Li and Y. Chen, *Opt. Mater. Express*, 2012, **2**, 814.
39. C. X. Guo, L. Y. Zhang, J. W. Miao, J. T. Zhang and C. M. Li, *Adv. Energy Mater.*, 2013, **3**, 167.
40. C. X. Guo and C. M. Li, *Energ. Environ. Sci.*, 2011, 4, 4504-4507.
41. Z. Z. Sun, D. K. James and J. M. Tour, *J. Phys. Chem. Lett.*, 2011, **2**, 2425.
42. Z. X. Chen, M. Zhou, Y. L. Cao, X. P. Ai, H. X. Yang and J. Liu, *Adv. Energy Mater.*, 2012, **2**, 95.
43. H. W. Hu, J. H. Xin and H. Hu, *Chempluschem*, 2013, **78**, 1483.
44. X. S. Wang, P. Huang, L. L. Feng, M. He, S. W. Guo, G. X. Shen and D. X. Cui, *Rsc Adv.*, 2012, **2**, 3816.
45. E. S. Abdel-Halim, M. H. El-Rafie and S. S. Al-Deyab, *Carbohyd. Polym.*, 2011, **85**, 692.
46. A. T. Paulino, M. R. Guilherme, A. V. Reis, G. M. Campese, E. C. Muniz and J. Nozaki, *J. Colloid Interf. Sci.*, 2006, **301**, 55.
47. L. L. Ren, T. X. Liu, J. A. Guo, S. Z. Guo, X. Y. Wang and W. Z. Wang, *Nanotechnology*, 2010, **21**, 335701 (7pp).
48. L. Feng, S. Zhang and Z. Liu, *Nanoscale*, 2011, **3**, 1252.
49. D. Z. Chen, H. Y. Quan, G. S. Wang and L. Guo, *Chempluschem*, 2013, **78**, 843.
50. I. Janowska, K. Chizari, O. Ersen, S. Zafeiratos, D. Soubane, V. Da Costa, V. Speisser, C. Boeglin, M. Houlle, D. Begin, D. Plee, M. J. Ledoux and C. Pham-Huu, *Nano Res.*, 2010, **3**, 126.
51. D. Li, M. B. Muller, S. Gilje, R. B. Kaner and G. G. Wallace, *Nat. Nanotechnol.*, 2008, **3**, 101.
52. B. Fei, B. T. Qian, Z. Y. Yang, R. H. Wang, W. C. Liu, C. L. Mak and J. H. Xin, *Carbon*, 2008, **46**, 1795.
53. J. F. Zhu, Y. J. Zhu, M. G. Ma, L. X. Yang and L. Gao, *J. Phys. Chem. C*, 2007, **111**, 3920.
54. A. M. S. Maia, H. V. M. Silva, P. S. Curti and R. C. Balaban, *Carbohyd. Polym.*, 2012, **90**, 778.
55. Z. M. Jin, Y. J. Pan, X. F. Li, M. L. Hu and L. Shen, *J. Mol. Struct.*, 2003, **660**, 67.
56. H. W. Hu and G. H. Chen, *Polym. Compos.*, 2010, **31**, 1770.
57. H. W. Hu, L. F. Chen and G. H. Chen, *Mater. Manuf. Process.*, 2011, **26**, 618.
58. R. Q. Liu, S. M. Liang, X. Z. Tang, D. Yan, X. F. Li and Z. Z. Yu, *J. Mater. Chem.*, 2012, **22**, 14160.
59. L. Y. Lu, H. L. Sun, F. B. Peng and Z. Y. Jiang, *J. Membrane Sci.*, 2006, **281**, 245.
60. Y. Chen, X. Zhang, P. Yu and Y. W. Ma, *Chem. Commun.*, 2009, **(30)**, 4527.
61. X. M. Yang, L. A. Li, S. M. Shang and X. M. Tao, *Polymer*, 2010, **51**, 3431.
62. M. R. Mohammadi and D. J. Fray, *Metall. Mater. Trans. A*, 2011, **42A**, 2481.
63. G. I. N. Waterhouse, G. A. Bowmaker and J. B. Metson, *Phys. Chem. Chem. Phys.*, 2001, **3**, 3838.
64. X. Z. Zhou, X. Huang, X. Y. Qi, S. X. Wu, C. Xue, F. Y. C. Boey, Q. Y. Yan, P. Chen and H. Zhang, *J. Phys. Chem. C*, 2009, **113**, 10842.
65. X. Z. Tang, X. F. Li, Z. W. Cao, J. L. Yang, H. Wang, X. Pu and Z. Z. Yu, *Carbon*, 2013, **59**, 93.
66. G. H. Jing, L. Wang, H. J. Yu, W. A. Amer and L. Zhang, *Colloid Surf. A*, 2013, **416**, 86.
67. C. Y. Liu, F. M. Wu, D. H. Yao, Y. Wang and Y. Q. Zhang, *Appl. Mech. Mater.*, 2012, **152**, 393.
68. P. Zhang, C. Shao, Z. Zhang, M. Zhang, J. Mu, Z. Guo and Y. Liu, *Nanoscale*, 2011, **3**, 3357.
69. S. W. Liu, R. J. Wehmschulte, G. D. Lian and C. M. Burba, *J. Solid State Chem.*, 2006, **179**, 696.
70. J. Li, C. Y. Liu and Y. Liu, *J. Mater. Chem.*, 2012, **22**, 8426.
71. X. Zhang and Z. H. Su, *Adv. Mater.*, 2012, **24**, 4574.
72. H. Li, S. Gan, D. Han, W. Ma, B. Cai, W. Zhang, Q. Zhang and L. Niu, *J. Mater. Chem. A*, 2014, **2**, 3461.
73. S. Saha, A. Pal, S. Kundu, S. Basu and T. Pal, *Langmuir*, 2010, **26**, 2885.
74. G. Fu, L. Ding, Y. Chen, J. Lin, Y. Tang and T. Lu, *CrystEngComm*, 2014, **16**, 1606.
75. A. S. Andrew, A. R. Schned, J. A. Heaney and M. R. Karagas, *Int. J. Cancer*, 2004, **109**, 581.
76. E. Pira, G. Piolatto, E. Negri, C. Romano, P. Boffetta, L. Lipworth, J. K. McLaughlin and C. La Vecchia, *J. Natl. Cancer I.*, 2010, **102**, 1096.
77. J. C. Fan, Z. X. Shi, M. Lian, H. Li and J. Yin, *J Mater Chem A*, 2013, **1**, 7433.
78. J. Z. Yi and L. M. Zhang, *Bioresource Technol*, 2008, **99**, 2182.
79. Z. J. Jiang, C. Y. Liu and L. W. Sun, *J. Phys. Chem. B*, 2005, **109**, 1730.
80. Y. X. Xu, K. X. Sheng, C. Li and G. Q. Shi, *Acs Nano*, 2010, 4, 4324.

Journal of Materials Chemistry A Accepted Manuscript

This journal is © The Royal Society of Chemistry 2012

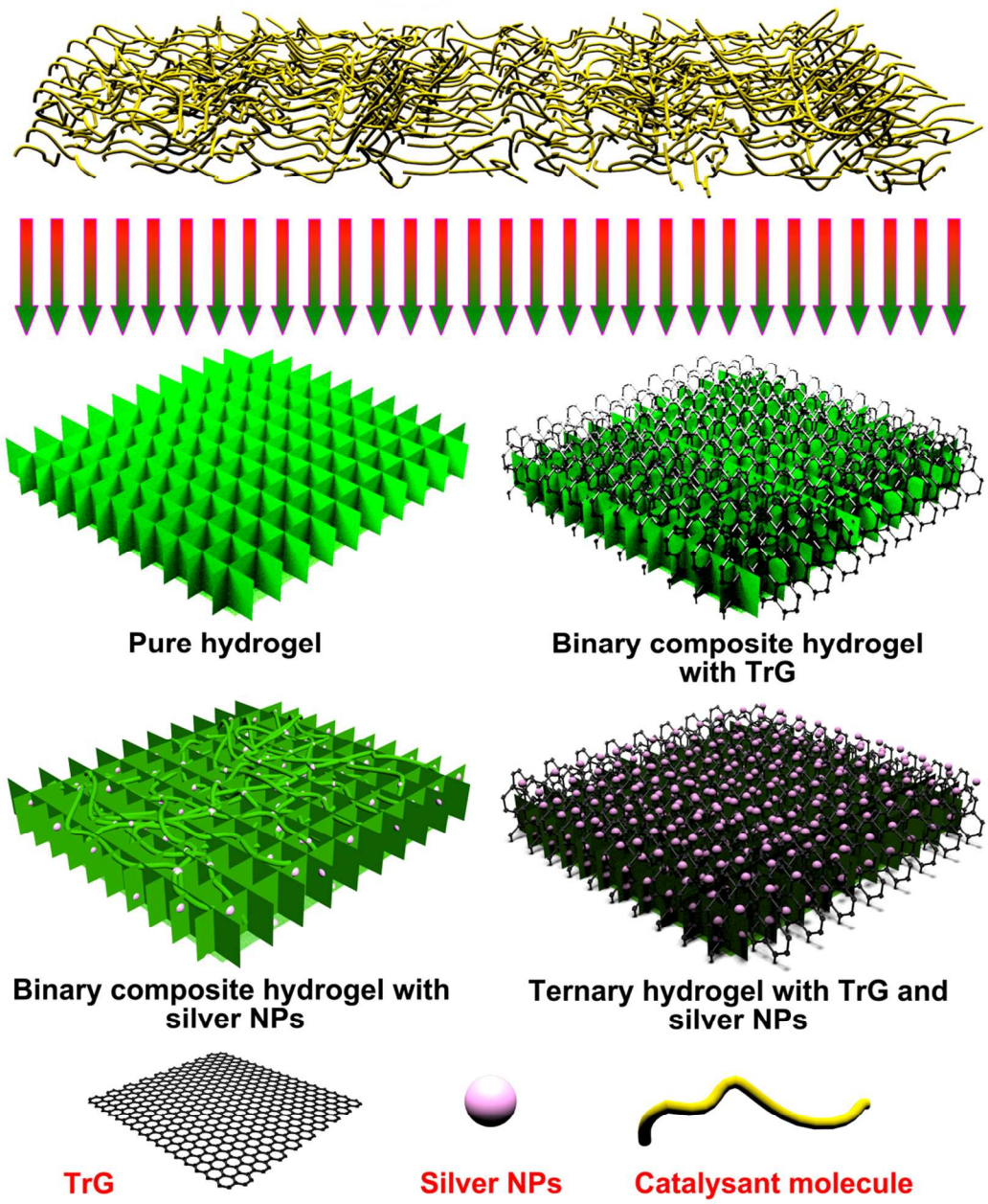

Scheme 1 Main content of the present study which includes preparation of PAM-based hydrogels with different compositions, catalysis investigation of these as-prepared hydrogels towards assisting chemical reduction of different kinds of catalysants, and explanation of the mechanism for the highly efficient catalytic performance.

Journal of Materials Chemistry A Accepted Manuscript

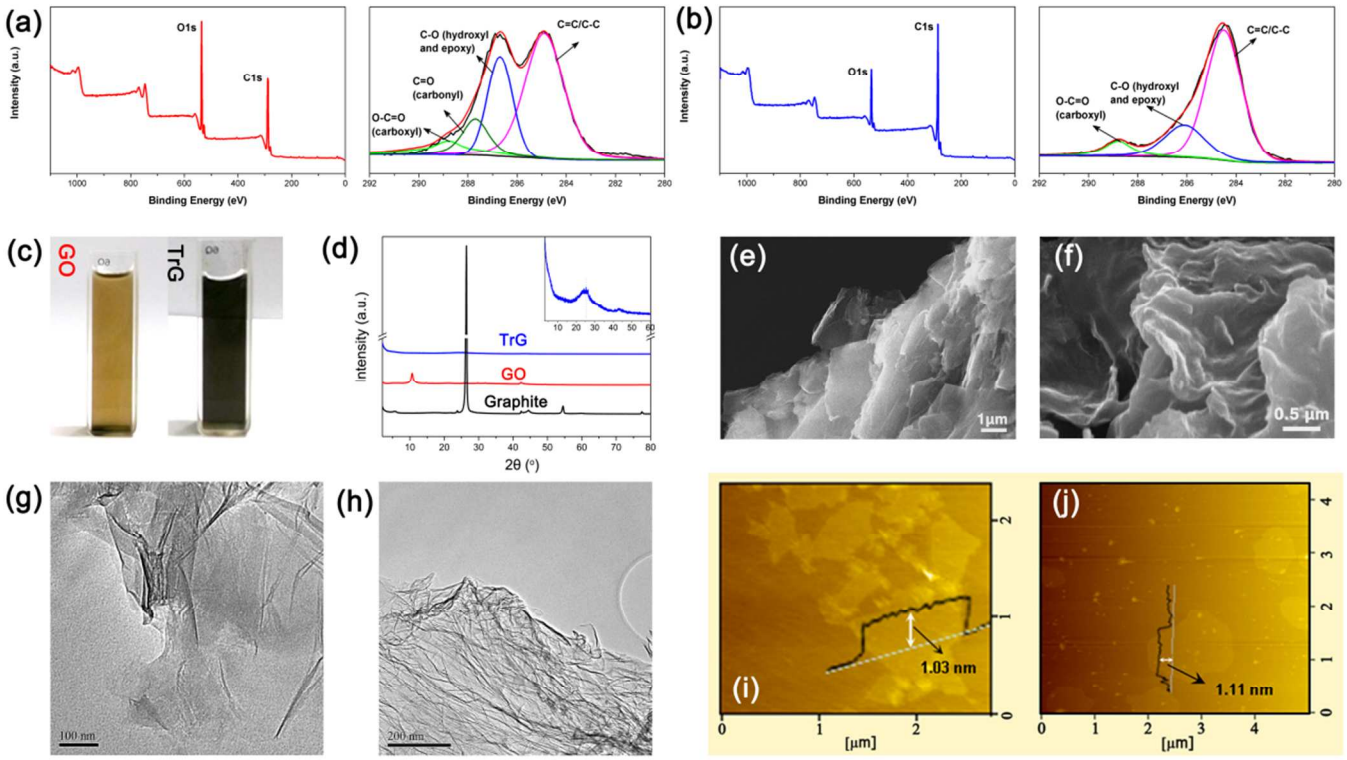

Fig. 1 Characterization of GO and TrG. (a) XPS survey and high-resolution XPS C 1s core-level spectra of GO. (b) XPS survey and high-resolution XPS C 1s core-level spectra of TrG. (c) photo images showing the water dispersions of GO and TrG. (d) XRD patterns of pristine graphite, GO and TrG (inset shows the magnified XRD curve of TrG). (e) SEM image of GO. (f) SEM image of TrG. (g) TEM image of GO. (h) TEM image of TrG. (i) AFM image coupled with height profile of GO. (j) AFM image coupled with height profile of TrG.

Journal of Materials Chemistry A Accepted Manuscript

This journal is © The Royal Society of Chemistry 2012

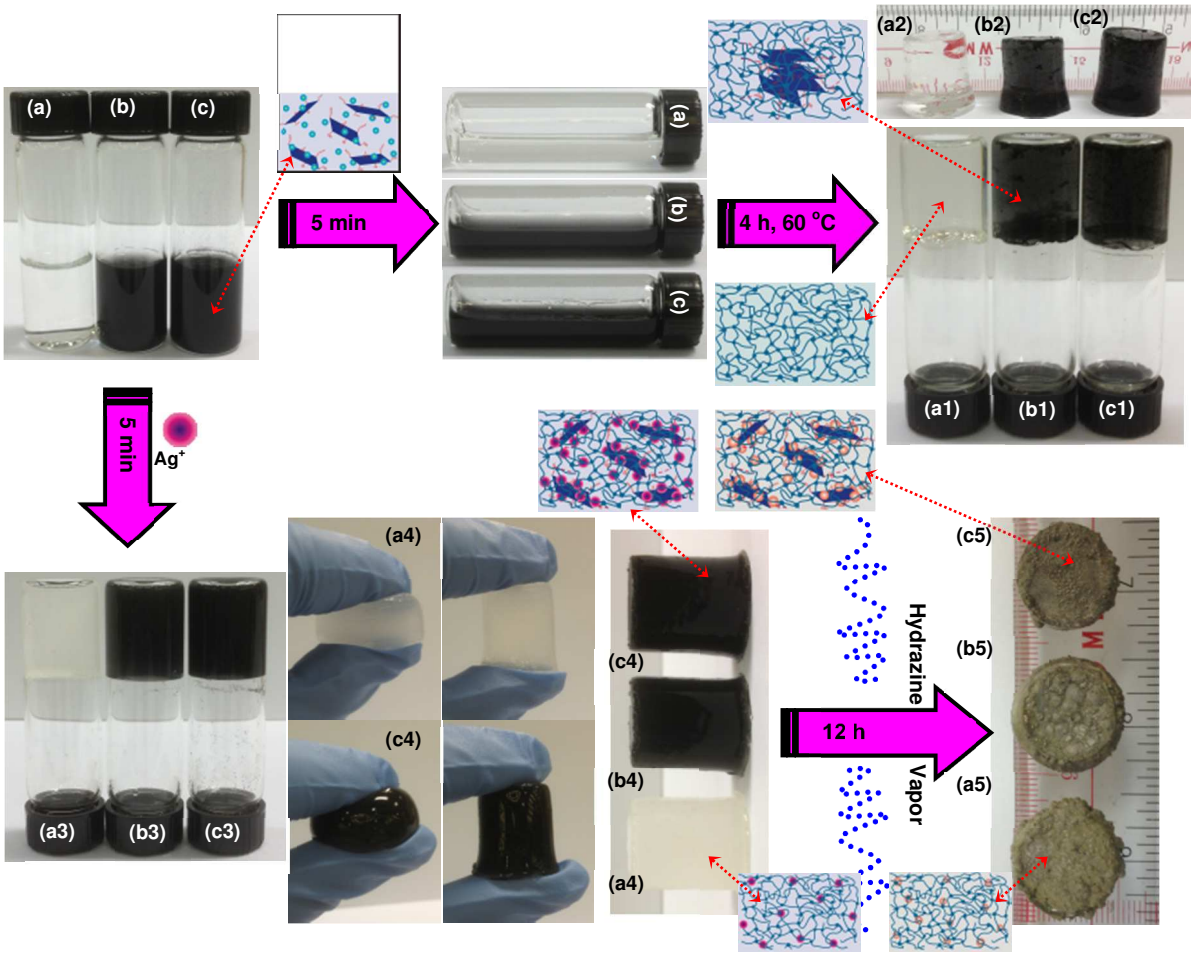

Fig. 2 Photo images and structural models revealing the main protocol of the present study. Preparation of pure PAM hydrogel and binary composite hydrogels PAM/0.6G and PAM/1.7G starting from the corresponding liquid solutions with monomer (a)-(c) to the resulting hydrogels (a1)-(c1), with the washed counterparts (a2)-(c2). Fabrication of binary composite hydrogel PAM/Ag^+ and ternary composite hydrogels PAM/0.6G/Ag^+ and PAM/1.7G/Ag^+ starting from the liquid solutions with monomer (a)-(c) to the resulting hydrogels (a3)-(c3), with the washed counterparts (a4)-(c4). The further reduction treatment of the hydrogels (a4)-(c4) with hydrazine vapor leads to the composite hydrogels (a5)-(c5), namely PAM/Ag, PAM/0.6G/Ag and PAM/1.7G/Ag. The proposed structural models of some typical samples are also shown accordingly as marked by dotted arrow line in red.

Journal of Materials Chemistry A Accepted Manuscript

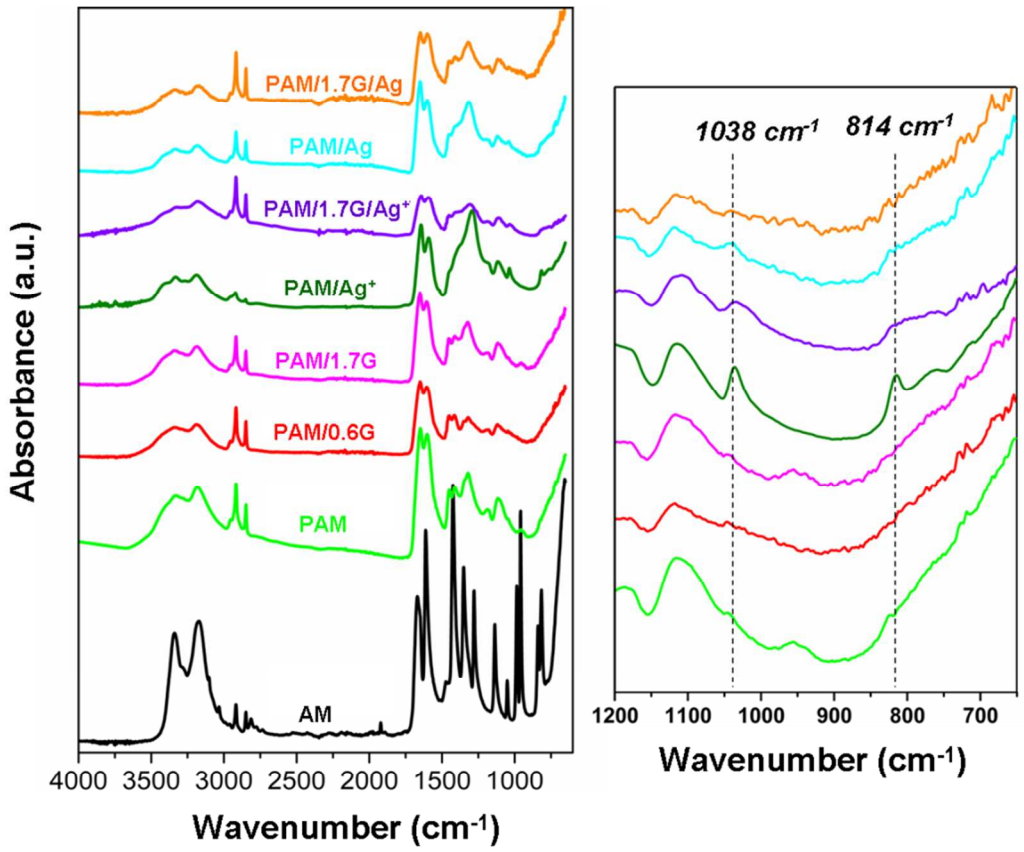

Fig. 3 FTIR spectra of the monomer AM, and oven-dried specimens of pure PAM hydrogel and various PAM-based composite hydrogels.

Journal of Materials Chemistry A Accepted Manuscript

This journal is © The Royal Society of Chemistry 2012

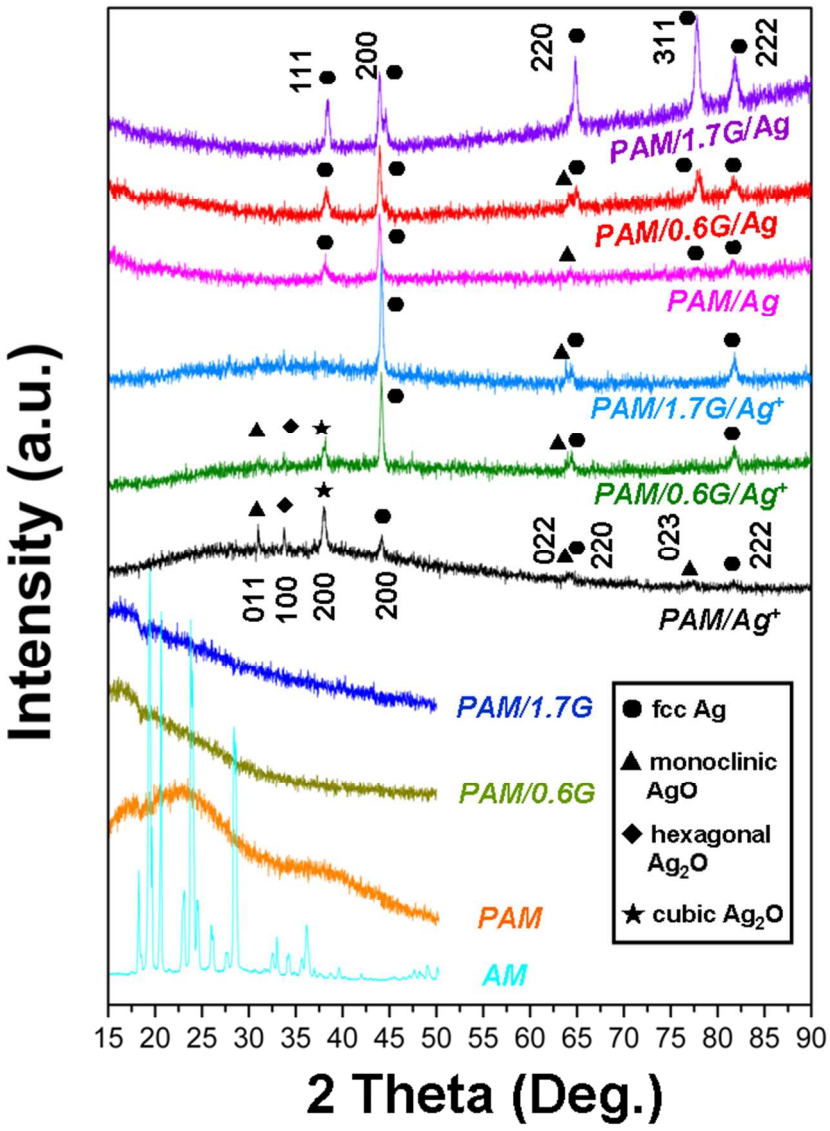

Fig. 4 XRD patterns of the monomer AM, and oven-dried specimens of pure PAM hydrogel and various PAM-based composite hydrogels.

Journal of Materials Chemistry A Accepted Manuscript

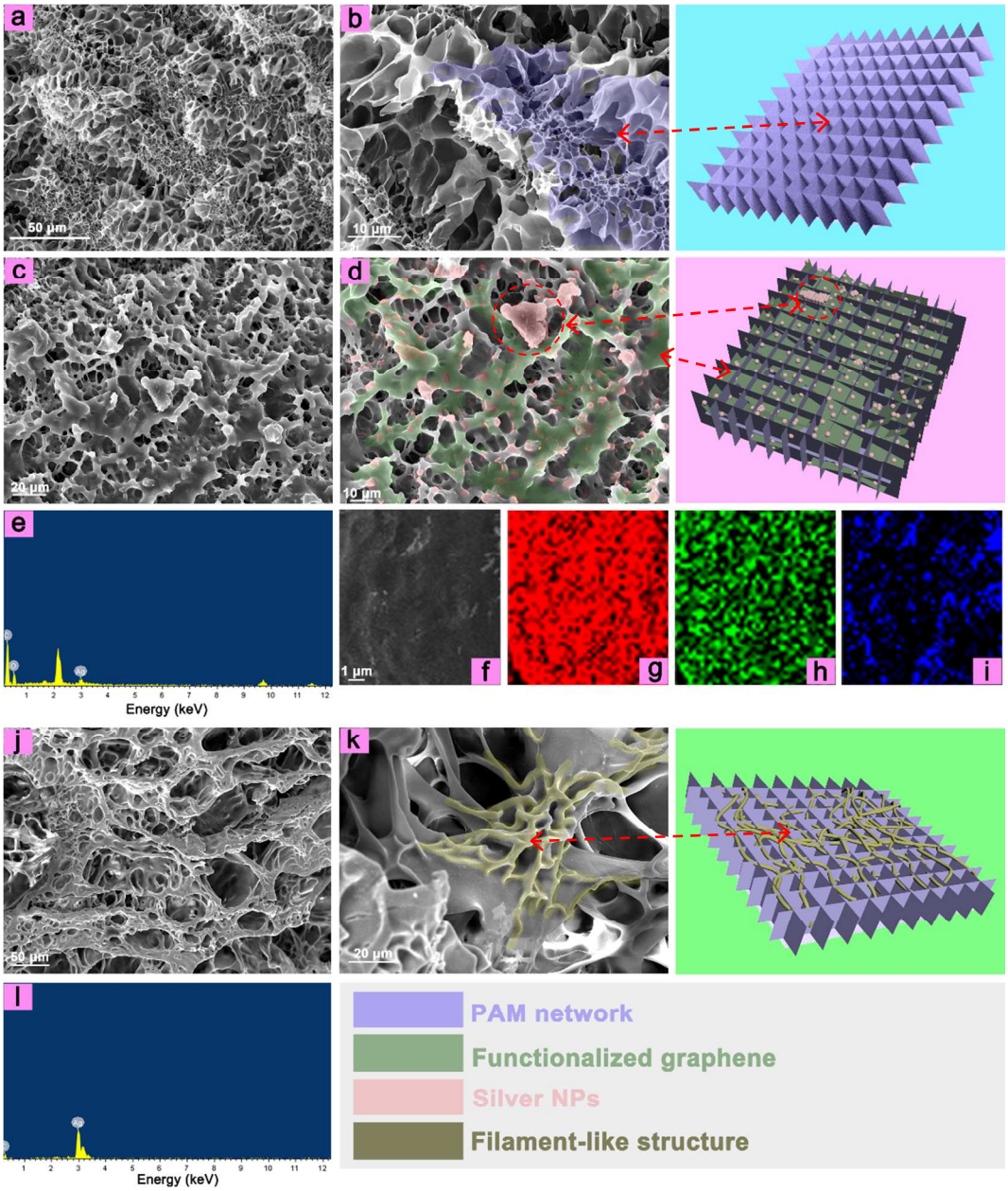

Fig. 5 Structure and cross-sectional morphology analysis for the lyophilized PAM-based hydrogel samples. SEM images of the freeze-fractured sections of the specimens prepared by lyophilizing the corresponding PAM-based hydrogel samples, including pure PAM hydrogel (a,b), ternary composite hydrogel, PAM/1.7G/Ag (c,d), and binary composite hydrogel, PAM/Ag (j,k); EDX spectra for PAM/1.7G/Ag (Fig. 5e) and PAM/Ag (Fig. 5l). EDX element mapping images of a sheet-like structure observable for PAM/1.7G/Ag (Fig. 5f: corresponding SEM image, Fig. 5g: element distribution of C Kα1, Fig. 5h: element distribution of O Kα1, and Fig. 5i: element distribution of Ag Lα1). Structure models of these samples are also provided, with the structural features indexed to those highlighted by the colour shadings in the corresponding SEM micrographs. Different colours are used to highlight the structural features, with the specific colour indication shown in the bottom right corner.

Journal of Materials Chemistry A Accepted Manuscript

This journal is © The Royal Society of Chemistry 2012

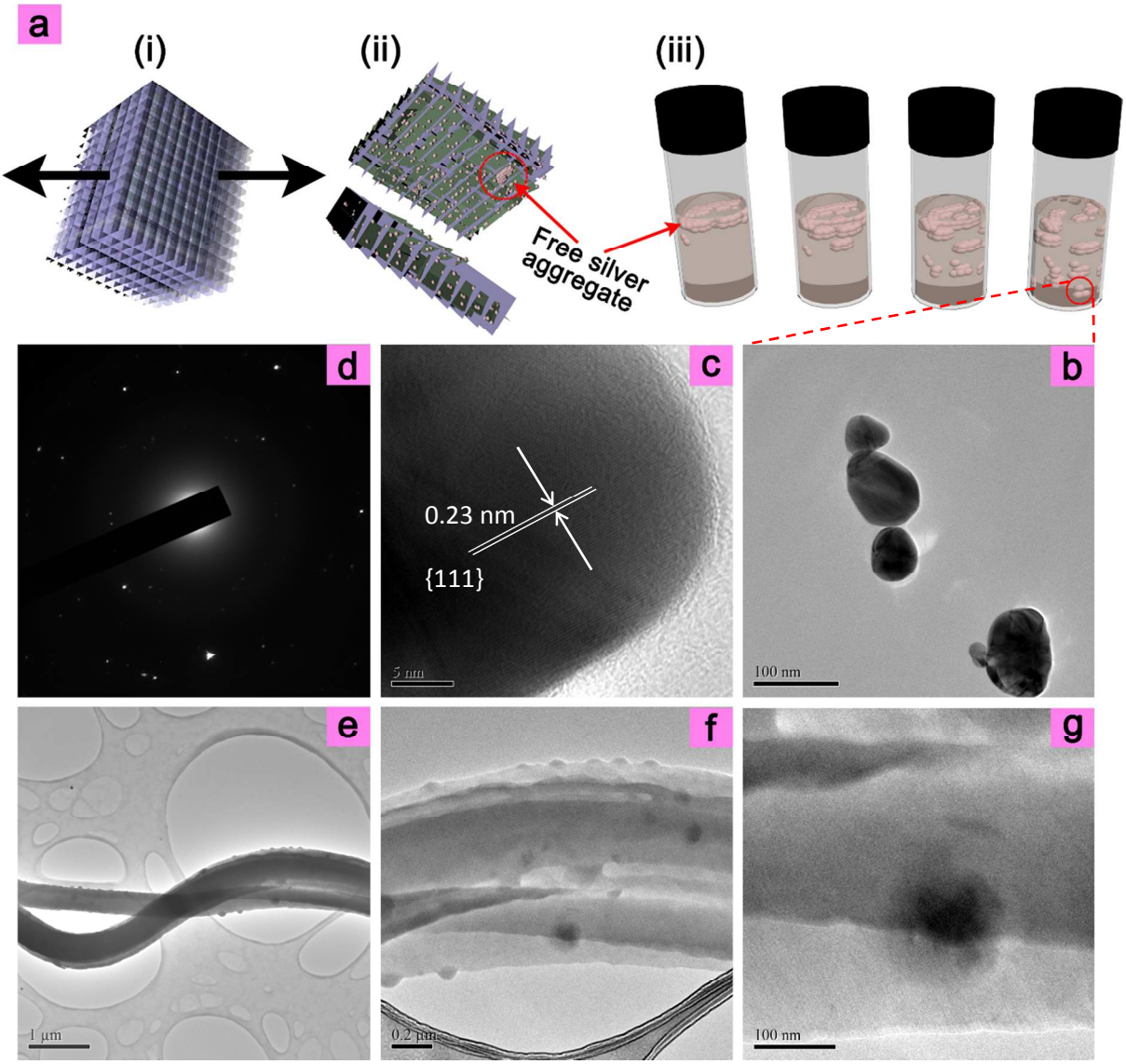

Fig. 6 Structure analysis of composite hydrogels by TEM test. (a) Schematic illustration of the release process of the silver aggregate free of bonding with TrG as demonstrated in the SEM images as for PAM/1.7G/Ag through the following steps: (i) pulling apart PAM/1.7G/Ag into several pieces; (ii) the split part with the exposed silver aggregate which was readily detached from the split parts due to the free of bonding interactions with TrG; (iii) dispersing the silver aggregate into water during which it disaggregated into some smaller particles. (b,c) TEM observation results for PAM/1.7G/Ag . (e-g) TEM observation results for PAM/Ag. (d) SAED pattern for the observed silver particles in Fig. 6c.

Journal of Materials Chemistry A Accepted Manuscript

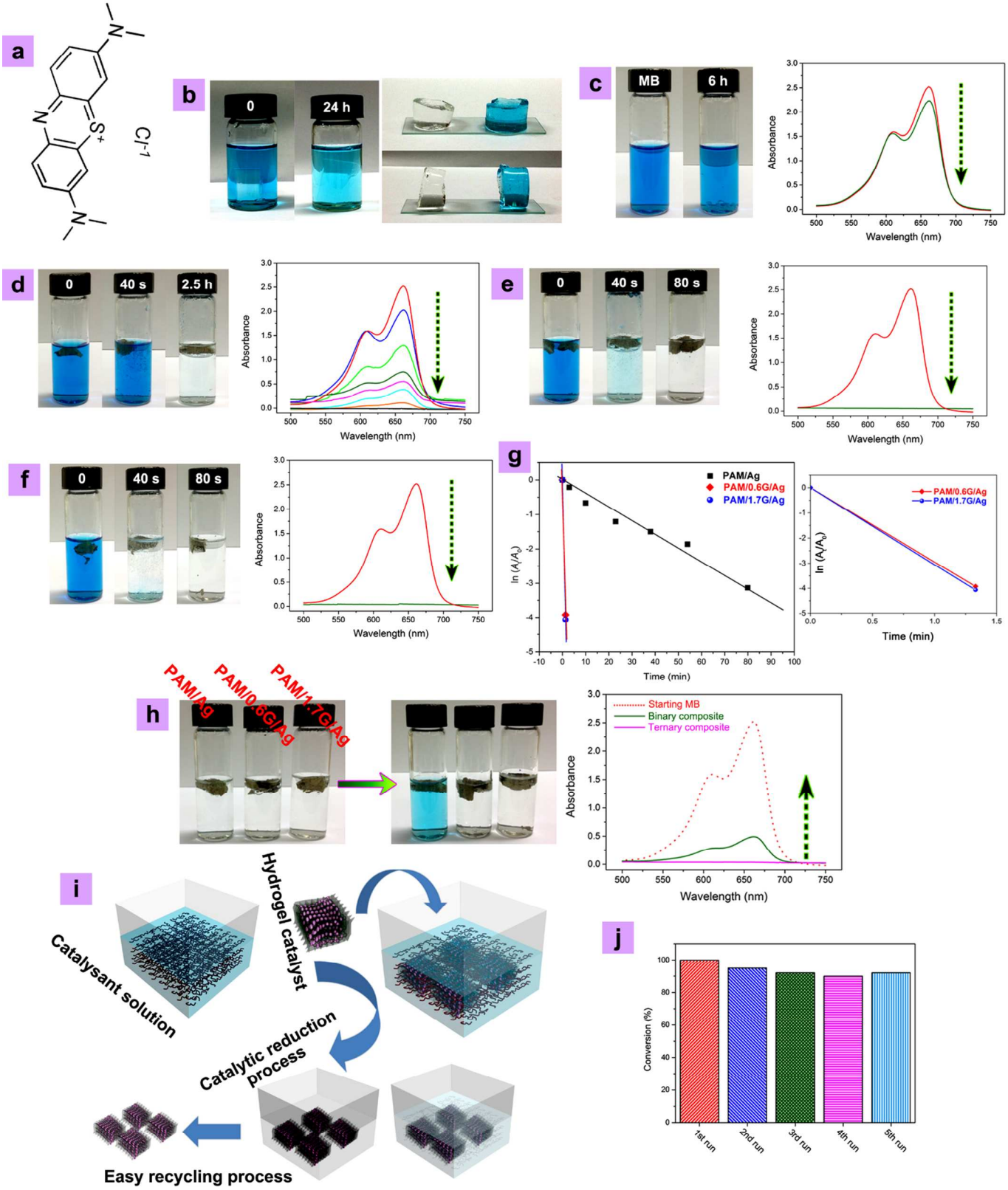

Fig. 7 Catalytic activity test results obtained by means of a model catalytic reduction of MB using $NaBH_4$ as the reducer and PAM-based hydrogel samples as the catalyst. (a) Molecular structure of MB. (b) Photo images showing the pure PAM hydrogel and its adsorption ability for MB. (c) Photo images and the corresponding UV/vis spectra revealing the very low reaction rate of the reaction between $NaBH_4$ and MB without the catalytic assistance. Photo images and the

Journal of Materials Chemistry A Accepted Manuscript

This journal is © The Royal Society of Chemistry 2012

corresponding UV/vis spectra showing the catalytic reduction with binary composite hydrogel, PAM/Ag (d), ternary composite hydrogel, PAM/0.6G/Ag (e), and ternary composite hydrogel, PAM/1.7G/Ag (f) as the catalyst. (g) The left Figure provides the plots of *ln* (A_t/A_0) against reaction time for the three reaction systems with PAM/Ag, PAM/0.6G/Ag and PAM/1.7G/Ag. The right Figure shows the corresponding magnified plots of ln (A_t/A_0) against reaction time for the systems with PAM/0.6G/Ag and PAM/1.7G/Ag. (h) Investigation of adsorption effect on discoloration of MB for PAM/Ag, PAM/0.6G/Ag and PAM/1.7G/Ag. (i) Schematic presentation of the overall catalytic reduction process and convenient handling property of the composite hydrogel samples. (j) Recyclability test for PAM/1.7G/Ag by repeated usage for five runs.

Journal of Materials Chemistry A Accepted Manuscript

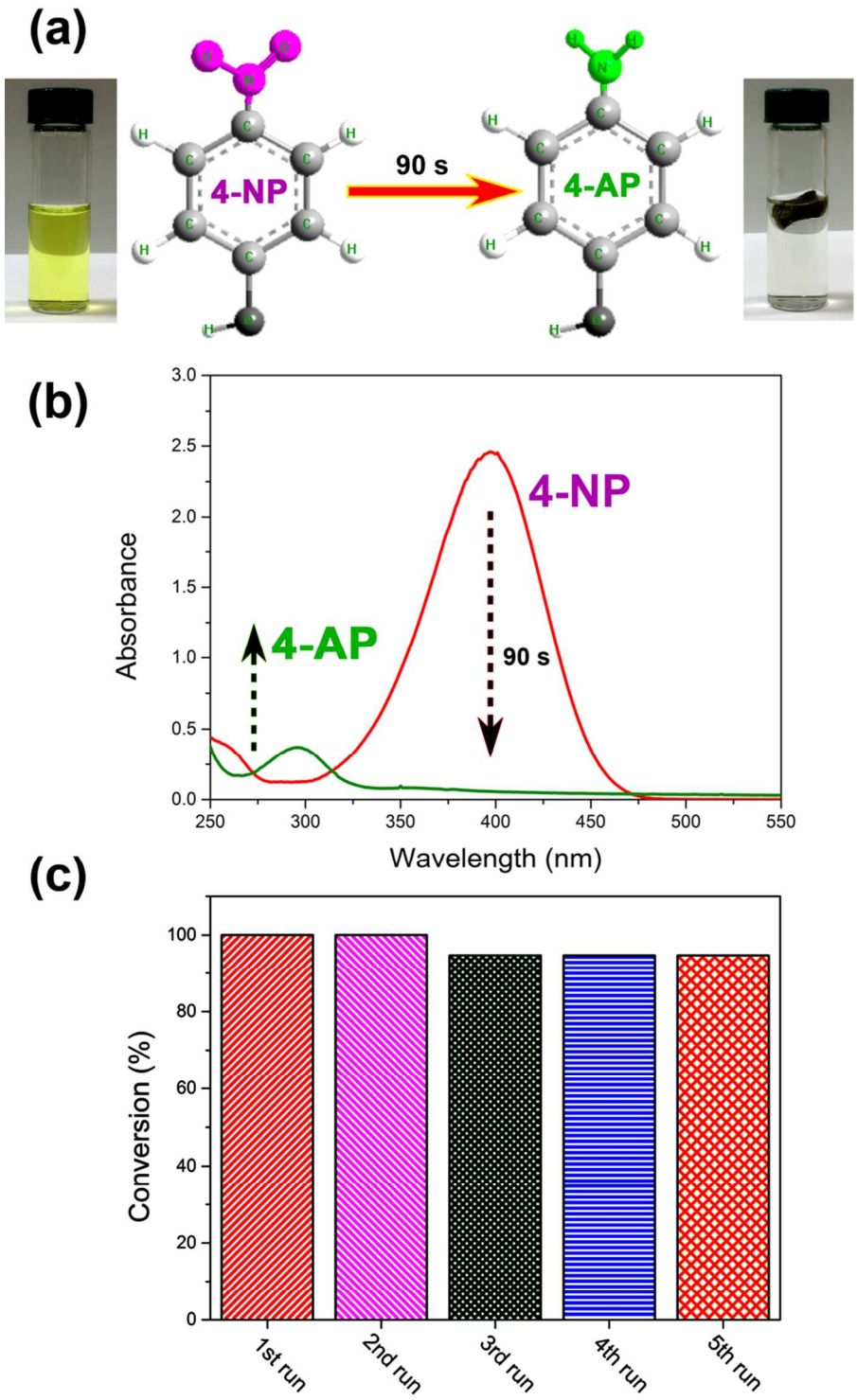

Fig. 8 Catalytic activity test results for the ternary composite hydrogel, PAM/1.7G/Ag, by a model reaction using an aromatic nitro compound, in this case 4-NP, as the catalysant. (a) Molecular structure models of 4-NP and its reduced product 4-AP, along with the photo images showing the water solutions before and after catalytic reduction with PAM/1.7G/Ag. (b) UV/vis spectra used to confirm the catalytic reduction of 4-NP which leads to 4-AP. (c) Recyclability test result for PMA/1.7G/Ag by five runs of repeated usage.

Journal of Materials Chemistry A Accepted Manuscript

This journal is © The Royal Society of Chemistry 2012

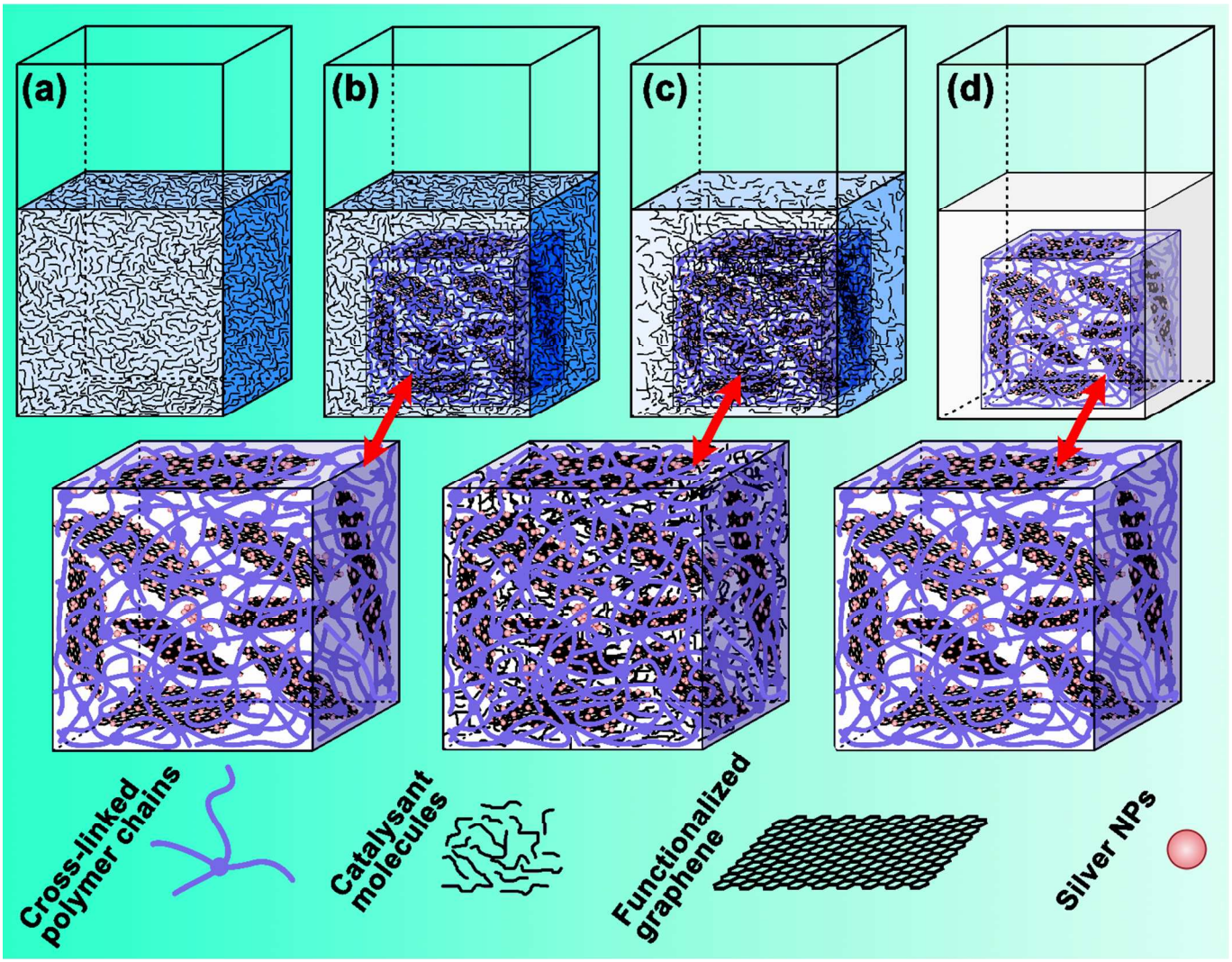

Scheme 2 Schematic illustration of the catalytic reduction process (from (a) to (d)) using our ternary composite catalyst. (a) The starting catalysant water solution. (b) Addition of the ternary composite to the solution. (c) Adsorption and catalytic reduction of the catalysant molecules. (d) The complete catalytic reduction and discoloration reaction. The state of the ternary composite during this process is highlighted by magnification, as indicated by the red arrow line.

Journal of Materials Chemistry A Accepted Manuscript

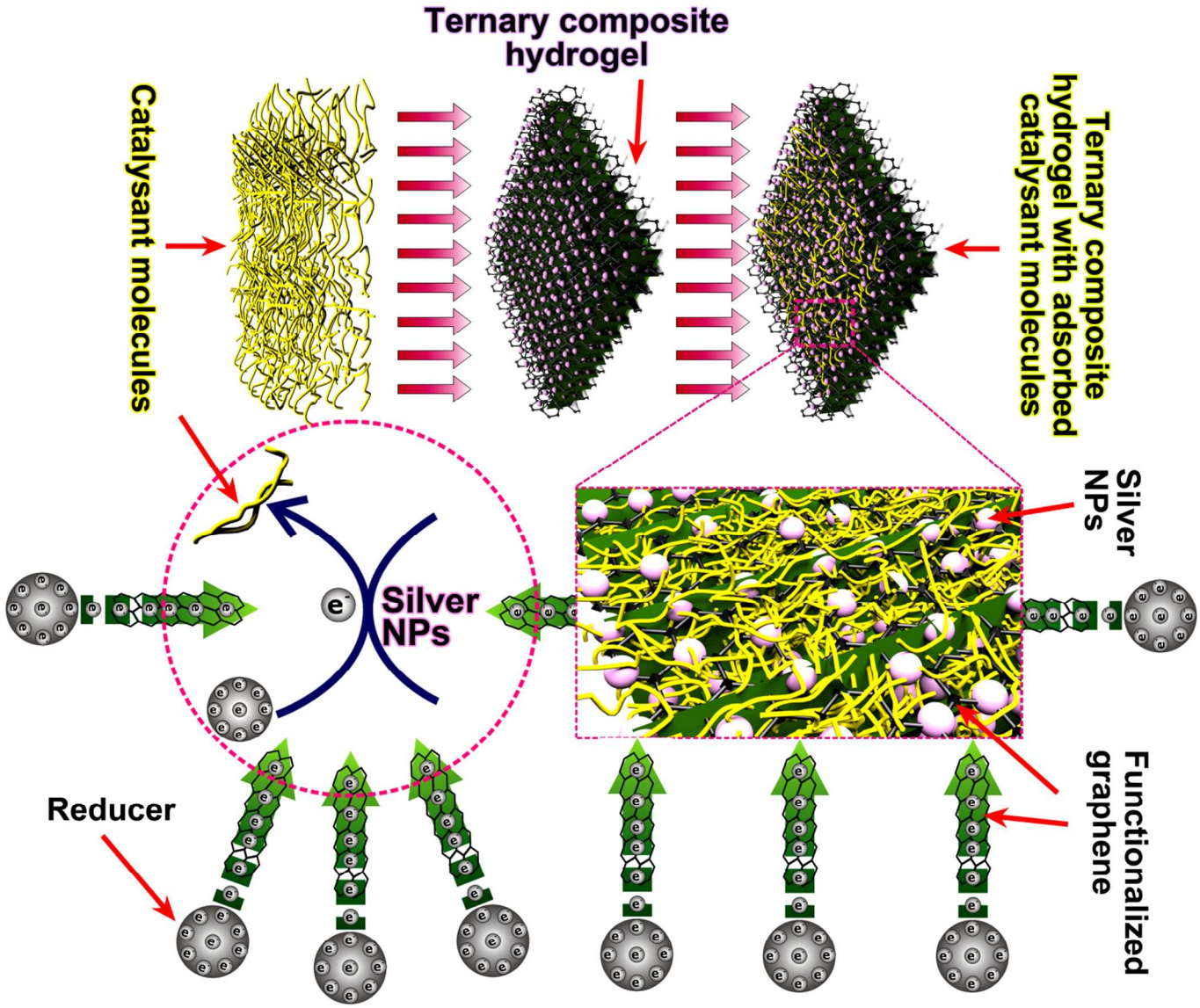

Scheme 3 Schematic explanation of extraordinary catalytic performance of the ternary composite hydrogel probably as a result of the synergistic effect of PAM polymer network with adsorption property, TrG having huge surface area and high electron mobility, and catalytically active silver NPs.

Journal of Materials Chemistry A Accepted Manuscript

This journal is © The Royal Society of Chemistry 2012